Available online at www.sciencedirect.com

SciVerse ScienceDirect

Physics Procedia 42 (2013) 163 – 170

Physics Procedia

PNCMI 2012 - Polarized Neutrons for Condensed Matter Investigations 2012

Neutron path length correction of a ^{3}He spin filter

W. C. Chen[a,b], R. Erwin[a], S. M. Watson[a]

[a]*National Institute of Standards and Technology, Gaithersburg, Maryland 20899 USA*
[b]*University of Maryland, College Park, Maryland 20742 USA*

Abstract

^{3}He neutron spin filters (NSF) have been widely used for polarized neutron instrumentation for worldwide neutron facilities. Here we report characterization of the two-dimensional neutron path variation of a ^{3}He NSF when a large divergent, scattered neutron beam passes through the end windows of a cylindrical ^{3}He cell. Path length variations of the transmission of the unpolarized neutrons through a ^{3}He NSF and neutron polarization produced from a ^{3}He NSF are characterized. We present a ray-tracing model to explain the path length variation and corresponding neutron transmission and neutron polarization variations, and compare the measured variations to those calculated from the model. Although the path length effect is not large, it should be corrected in the polarization efficiency correction software when a ^{3}He NSF is used for SANS polarization analysis. The path length variation effect can be adopted to other types of neutron scattering spectrometers when using ^{3}He NSFs.

Selection and peer-review under responsibility of the Organizing Committee of the 9th International Workshop on Polarised Neutrons in Condensed Matter Investigations

Keywords: ^{3}He NSF, path length variation

1. Introduction

Recent years have witnessed the rapidly expanding applications of ^{3}He neutron spin filters (NSF) in various polarized neutron instrumentation such as the triple-axis spectrometer (TAS) [1], the small-angle neutron scattering (SANS) instrument [2, 3, 4], the reflectometer [5, 6], and wide-angle polarization analysis [7, 8]. A ^{3}He neutron spin filter (NSF) is based on the strong spin dependence of the neutron absorption cross section for ^{3}He and is a transmission-based neutron polarizing device. Polarized neutronic performance of a ^{3}He NSF is governed by the ^{3}He gas polarization, gas thickness (product of the neutron path length and ^{3}He density), and wavelength, and is predictable and calculable once the parameters above are known. Unlike a supermirror polarizing device, the performance yielded by a ^{3}He NSF is spatially uniform if the gas thickness is uniform.

Spin-exchange optical pumping (SEOP) based ^{3}He cells for neutron scattering applications have been commonly fabricated from boron-free aluminosilicate glass GE180 [9]. It has been found [10, 11] that long relaxation times are obtained with greater reliability for cells made from fully blown glass. For this reason,

[1]Email: wcchen@nist.gov (W.C. Chen)

Selection and peer-review under responsibility of the Organizing Committee of the 9th International Workshop on Polarised Neutrons in Condensed Matter Investigations
doi:10.1016/j.phpro.2013.03.191

blown cells are employed whenever possible in SEOP applications. To protect the cell from rupture and for practical reasons, the cell windows for the neutron pathway are often made to be curved. Whether the neutron path length is spatially uniform or not depends on the ^{3}He cell geometry design and fabrication technology limitation. Although the path length can be spatially uniform as in the case of banana-shaped cells used for wide angle polarization analysis [7, 12], the path length of ^{3}He NSFs are often not uniform for applications in SANS, TAS and reflectometry. Therefore the path length variation should be corrected for use on various beam-lines.

SANS is equipped with a large two-dimensional position-sensitive detector (PSD) and is well suited for characterization of neutron path length variation of a ^{3}He NSF cell. Polarization analysis in SANS with a ^{3}He NSF [3, 13] has recently been employed for studies of magnetic nanoparticles [2, 14], an exchanged-biased system [15], a ferroelectric material [16], bio-nanomagnetism [17], and a giant magnetostrictor [18]. These experiments required careful attention to polarization corrections, which result from the imperfection of the ^{3}He spin filters, precession coil spin flipper, and possible spin transport. Spatially homogeneous polarization efficiency is necessary in performing polarization analysis, especially in probing a weak magnetic signal from the sample, as shown in reference [14] where uncertainties of polarization efficiencies over 1 % would mask the expected weak magnetic features. Hence, accurate knowledge of the spatial variation of the neutron path length and corresponding polarized neutronic performance of a ^{3}He NSF is essential. Here, we report a model for the neutron path length variation and the corresponding transmission and neutron polarization variations measured with unpolarized neutrons in SANS. A model and experimental characterization of the spatial variations in polarized neutronic performance measured with polarized neutrons will be shown in a future publication.

2. Polarized ^{3}He spin filter as a spin analysis device

A ^{3}He neutron spin filter is a transmission-based neutron-polarizing device. It relies upon the strong spin dependence of the cross section for neutron absorption by ^{3}He gas, which arises from the resonance reaction ^{3}He$(n,p)^3$H (absorption cross section $\sigma+ = \sigma\uparrow\uparrow \approx 0$ when the neutron spin is parallel to the ^{3}He spin; while $\sigma- = \sigma\downarrow\uparrow \approx 10666$ b at 1.8 Å when the neutron spin is anti-parallel to the ^{3}He spin). The transmission for an unpolarized neutron beam passing through a polarized ^{3}He cell is given by

$$T_{\mathrm{n}} = T_0 \cosh\left(\sigma n l P_{\mathrm{He}}\right) \tag{1}$$

P_{He} is the ^{3}He polarization. σnl is the opacity of the cell, which is linearly proportional to the ^{3}He gas density (n), the absorption cross section σ ($\propto$ wavelength λ), and the length (l) of the cell. T_0 is the transmission for an unpolarized neutron beam passing through an unpolarized ^{3}He cell and is given by

$$T_0 = T_{\mathrm{E}} \exp\left(-\sigma n l\right) \tag{2}$$

where T_{E} is the glass or silicon window transmission of the ^{3}He cells. Often the SEOP ^{3}He cells are fabricated from GE-180 glass. We had a window thickness of about 7 mm for ^{3}He cells in SANS application and typically observed T_{E} of 0.87. The wavelength dependence of the transmission of glass cell windows has been measured to be relatively flat [19]. The resulting neutron polarization after a polarized ^{3}He cell for an unpolarized beam is given by

$$P_{\mathrm{n}} = \tanh\left(\sigma n l P_{\mathrm{He}}\right) = \sqrt{1 - \frac{T_0^2}{T_{\mathrm{n}}^2}} \tag{3}$$

3. Modeling the neutron path length variation

The neutron path length variation comes from the non-flatness of the ^{3}He cell windows and the geometric effect of the instrument setup. To model the spatial variation, the end-window can be characterized as part of a spherical object with radius of curvature, R (R approaches infinity for flat windows). In order to model

this, we take the coordinate system origin at the center of the ^{3}He cell as shown in Fig. 1. Any scattered neutron ray that passes through the cell intersects both the front and back spherical windows of the ^{3}He cell. Then the coordinates of the intersecting points are calculated. A neutron path length corresponding to that scattered ray is the length between two intersecting points. Given any pixel on a two-dimensional SANS position sensitive detector (PSD), the scattering angle 2θ is known, hence we can average the cell path length over the sample area (typically a disc) assuming the sample is uniformly illuminated in the incident beam. Let $D_{\rm sc}$ be the distance from the sample to the analyzing ^{3}He cell center, and $D_{\rm cd}$ be the distance of the ^{3}He cell center to the detector. Then the distance from the sample to the detector, $D_{\rm sd}$, is $D_{\rm cd} + D_{\rm sc}$. Therefore for any given pixel with its subtending scattering angle 2θ, the neutron path length l integrated over the sample area can be expressed as

$$\frac{l}{l_0} \simeq 1 + \left[\frac{1}{2}\left(1 - \frac{l_0}{2R}\right) - \frac{D_{\rm sc}^2}{Rl_0}\right]\tan^2(2\theta) + \left[\frac{1}{2}\left(1 - \frac{l_0}{2R}\right) - \frac{D_{\rm cd}^2}{Rl_0}\right]\frac{A_{\rm S}}{2\pi D_{\rm sd}^2} \tag{4}$$

where $A_{\rm S}$ is the sample cross sectional area. l_0 is the neutron path length via the cell center and is typically measured with a small neutron beam. Generally, the term $\frac{1}{2}\left(1 - \frac{l_0}{2R}\right)$ is much smaller than the term $\frac{D_{\rm cd}^2}{Rl_0}$ since $D_{\rm cd}$ is much larger than R and l_0, thus, Eq. 4 can be rewritten as

$$\frac{l}{l_0} \simeq 1 + \left[\frac{1}{2}\left(1 - \frac{l_0}{2R}\right) - \frac{D_{\rm sc}^2}{Rl_0}\right]\tan^2(2\theta) - \frac{D_{\rm cd}^2}{Rl_0}\frac{A_{\rm S}}{2\pi D_{\rm sd}^2} \tag{5}$$

Given the fact that the sample area is much smaller than the product of R and l_0, the last term in Eq. 5 is typically negligible. To make a straightforward evaluation, $\frac{D_{\rm sc}^2}{Rl_0}$ in our typical SANS setup is much larger than $\frac{1}{2}\left(1 - \frac{l_0}{2R}\right)$, hence $\frac{l}{l_0}$ can be approximated by $1 - \frac{D_{\rm sc}^2}{Rl_0}\tan^2(2\theta)$. This implies that $\frac{l}{l_0}$ decreases as the scattering angle and the distance from the sample to the cell increases, as the curvature of the cell window and the cell length decreases. For a flat windowed cell [11, 20], $\frac{l}{l_0} \simeq 1 + \frac{1}{2}\tan^2(2\theta)$. This is consistent with the exact path length correction for flat windows where $\frac{l}{l_0} = \frac{1}{\cos(2\theta)}$. So the neutron path length in this case weakly increases with the scattering angle.

4. Experiment setup

The experiments were performed at the National Institute of Standards and Technology Center for Neutron Research on the NG-3 SANS beam-line. The NG-3 SANS detector has 128 pixels by 128 pixels with a 5 mm pixel resolution. To extend the momentum transfer range, a wavelength of 5 Å was chosen. The neutron transmission-based ^{3}He polarization measurement commonly utilizes a small direct beam or a small diffracted beam [1]. In this case, only a single value of the opacity is obtained, often through the cell center. To map the spatial variation of the neutron path length, we have utilized the small angle scattering from a strong scatterer as a measurement probe. Since the transmission through an unpolarized ^{3}He cell is about 0.045 at an opacity value of 3, the intensity differs by a factor of 22 for the transmission measurements with no cell and unpolarized cell. Consequently, it is essential to use a sample that produces strong coherent scattering (A coherent scatterer is necessary for future characterization of the spatial variation of the polarized neutronic performance). Therefore a glassy carbon sample [21] was chosen. A ^{3}He cell was placed after the glassy carbon sample to simulate a routine SANS polarization analysis setup [2]. Three SANS measurements were done to characterize the spatial variation of a ^{3}He NSF for an unpolarized neutron beam: (1) no ^{3}He cell in the beam; (2) a polarized ^{3}He cell in the beam; (3) an unpolarized cell in the beam. For all three measurements, the data are corrected for detector efficiency, empty, and background as described in the reference [22]. The time dependence of the ^{3}He polarization was also corrected. Even with the glassy carbon sample, a long counting time on the order of one hour is necessary to achieve good counting statistics pixel by pixel for the unpolarized ^{3}He cell measurement.

For the experiment, ^{3}He gas was polarized offline in one of the NIST state-of-the-art SEOP systems [11], then transported to the NG-3 SANS beam-line. During the experiment, the ^{3}He polarization was maintained

in a compact, magnetically shielded solenoid that is 25 cm diameter and 35 cm long, and provides a volume-average transverse field gradient of $|\vec{\nabla}B_\perp/B| \approx 6\times10^{-4}$ cm^{-1} even with a 1.6 T electromagnet operating nearby (not necessary for the test here, but it is required for future characterization for the polarized beam setup). The ^{3}He polarization relaxation time was about 200 h, long enough as compared to an one-hour counting time. The ^{3}He cell was under vacuum and typically about 50 cm away from the sample when using the 1.6 T electromagnet applied to the sample. To verify cancellation of the path length variation effect on the scattering angle as shown in Eq. 5 (see discussion in Sec. 5), we used a different experiment setup where a ^{3}He analyzer cell was located only several centimeters away from the glass carbon sample with both the sample and cell placed near the center of a pair of 55 cm diameter Helmholtz coils. The Helmholtz coils serve as the sample field and also provide a uniform field to maintain the ^{3}He polarization.

5. Experimental results

We began with the standard experiment setup where the ^{3}He cell Burgundy was placed 52 cm away from the sample, with a sample-to-detector distance of 402 cm. We have measured the path length variations of T_0 (opacity), T_n, P_n, and ^{3}He polarization pixel by pixel on a SANS 2D PSD. Shown in Fig. 2 is a SANS image with the polarized cell Burgundy, clearly indicating the measurable Q ($Q = \frac{4\pi}{\lambda}\sin(\theta)$) range set by the magnetically shielded solenoid where the neutron shielding material is matched to the mu-metal end cap hole. Fig. 3 shows the opacity variation at different scattering angles (converted to Q space) obtained using Eq. 2. The opacity decreases by about 10 % from the cell center to the edge, in good agreement with the calculated opacity variation modeled for the cell Burgundy with a radius of curvature of 20 cm. The radius of curvature was determined by fitting the model to the measurements. The sudden change of the opacity at $Q = 0.094$ Å^{-1} indicates the Q limit described in Fig. 2. Error bars in all figures are obtained from counting statistics, and represent one standard deviation.

Fig. 4 shows the variation of the transmission of the polarized ^{3}He for the cell Burgundy vs the wave vector transfer obtained using Eq. 1 at a ^{3}He polarization of 0.754 (see Fig. 6). The transmission increases by about 8 % from the cell center to the edge, in good agreement with the calculated variation in transmission. The neutron polarization is not affected from a moderate variation in opacity and decreases only by less than 1 % from the cell center to the edge as shown in Fig. 5. Fig. 6 shows the ^{3}He polarization variation obtained using Eq. 3 and the path length variation obtained in Fig. 3. Best fit of the ^{3}He polarization plot to a constant yielded a ^{3}He polarization value of 0.754. ^{3}He polarization was also measured directly from the transmission measurement using Eqs. 1, 2, 3 and determined to be 0.752±0.008 with a small correction applied for the polarization decay due to the long counting time of the scattering measurement. As expected, the ^{3}He gas polarization is independent of the scattering angle and should be spatially uniform. The experiment started with the empty measurement (no glassy carbon sample) that is required for a SANS measurement followed by a 12 h polarization decay of the cell Burgundy before the T_n transmission measurement. The initial ^{3}He polarization was 0.800±0.008 for the cell Burgundy.

From Eq. 5, it is possible to cancel the $\tan^2(2\theta)$ dependence of the path length, i.e., the $\tan^2(2\theta)$ dependence vanishes by choosing an appropriate value of D_{sc} such that

$$\frac{l_0}{2}\left(R - \frac{l_0}{2}\right) = D_{sc}^2 \tag{6}$$

Generally, it would be necessary to locate the cell very close to the sample to satisfy Eq. 6. For example, for the cell Maverick, $l_0 = 6.2$ cm and $R = 25$ cm. This would imply D_{sc}=8.2 cm. To perform the test, we used a pair of Helmholtz coils to maintain the ^{3}He polarization, and placed the cell Maverick front window only 5.1 cm away from the glassy carbon sample. The sample-to-detector distance was 351 cm. We then repeated the three measurement sequences as used for the cell Burgundy. The results are shown in Figs. 3, 4, 5, 6. Plots of the opacity, T_n, and P_n vs Q are flat for the entire Q range, indicating that they are independent of the scattering angle, in good agreement with the ray-tracing model. Given that the cell is large in diameter and close to the sample, there is no limit in maximum achievable Q by the cell. The Q limit is set only by the size of the silicon window attached to the vacuum sample chamber.

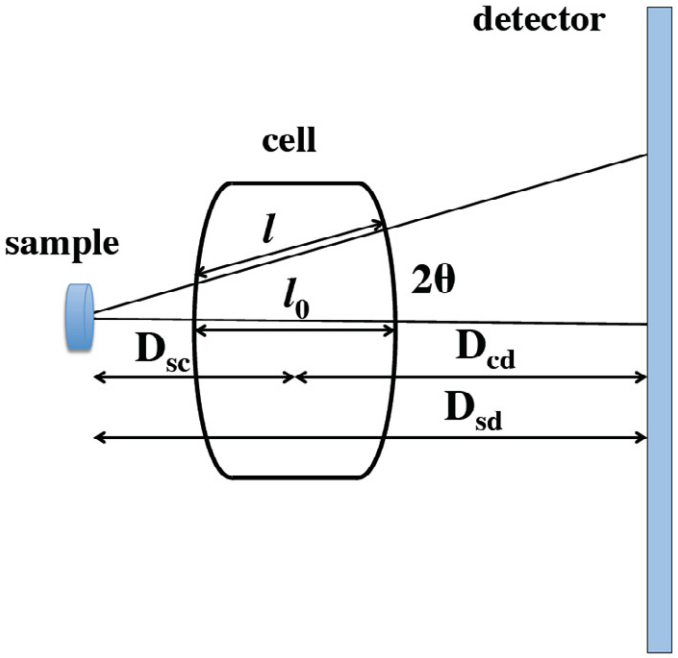

Fig. 1. Schematic diagram for modeling the neutron path length variation in a SANS geometry. D_{sc} is the distance from the sample to the ^{3}He cell center. D_{cd} is the distance of the ^{3}He cell center to the detector. D_{sd} is the distance of the sample to the detector. l_0 is the neutron path length via the cell center. l is the neutron path length, corresponding to a pixel (2θ) on the 2-D PSD.

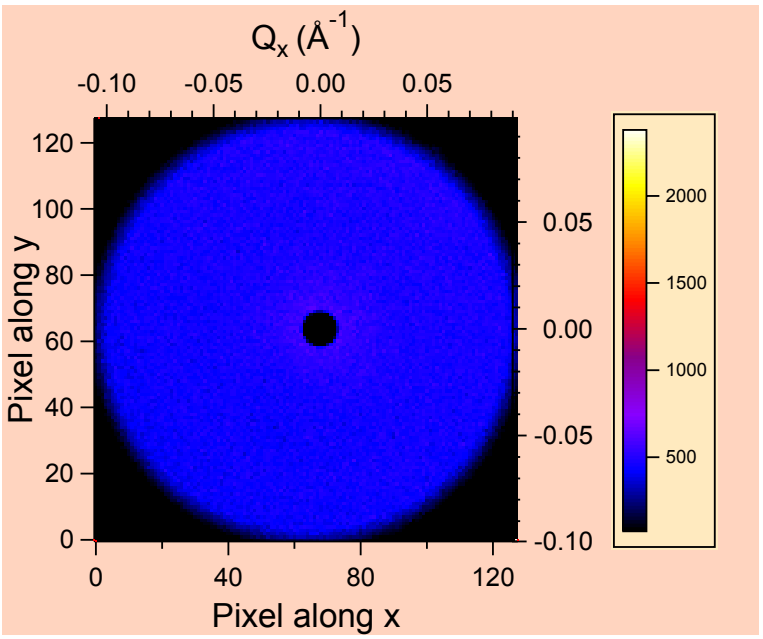

Fig. 2. SANS image for the polarized cell Burgundy after corrections for detector efficiency, empty and background. The right axis is the wave vector transfer (Q_y in Å^{-1}) along y. The circle indicates the Q limit from the mu-metal end cap hole of the magnetically shielded solenoid where the neutron shielding material is attached.

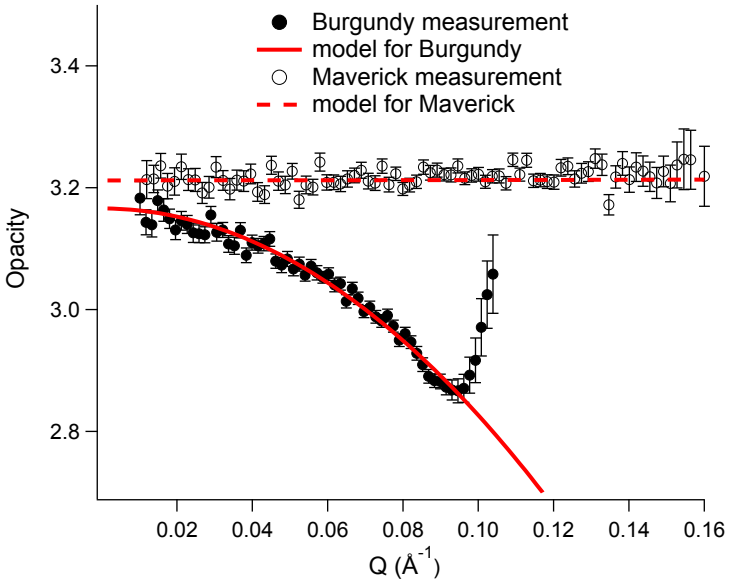

Fig. 3. Path length variation in opacity as a function of the wave vector transfer for the cell Burgundy (solid circles) and Maverick (open circles). The calculated variations were done for the cell Burgundy (solid line) and Maverick (dash line). The modeling was done for the cell Burgundy with R = 20 cm, D_{sc} = 52 cm, D_{cd} = 350 cm, and for the cell Maverick with R = 25 cm, D_{sc} = 8.2 cm, D_{cd} = 343 cm. The transmissions (T_E) of cell windows were determined to be 0.86 for the cell Burgundy and 0.87 for the cell Maverick based on the average wall thickness and T_E measurements of other similar cells.

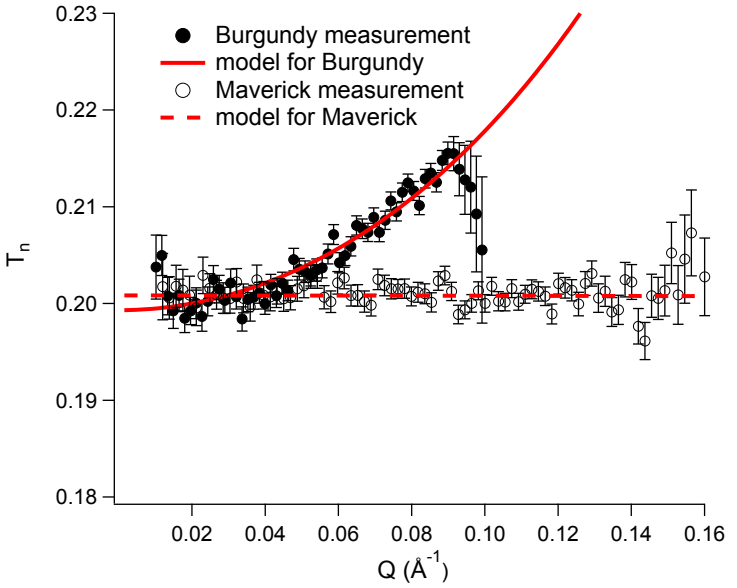

Fig. 4. Path length variation in T_n as a function of the wave vector transfer for the cell Burgundy (solid circles) and Maverick (open circles). The calculated variations were done for the cells Burgundy (solid line) and Maverick (dash line). ^{3}He polarizations were determined to be 0.754 and 0.757 for the cell Burgundy and Maverick, respectively (see details in text).

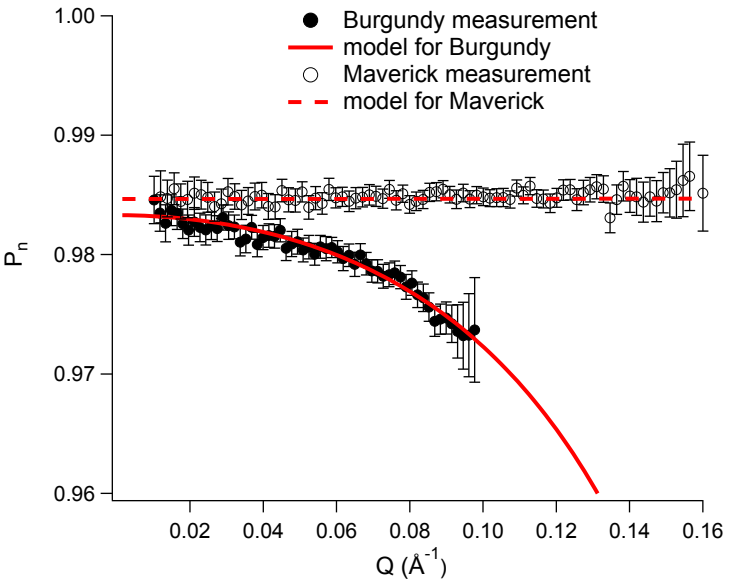

Fig. 5. Path length variation in P_n as a function of the wave vector transfer for the cell Burgundy (solid circles) and Maverick (open circles). The calculated variations were done for the cell Burgundy (solid line) and Maverick (dash line). ^{3}He polarizations were determined to be 0.754 and 0.757 for the cell Burgundy and Maverick, respectively (see details in text).

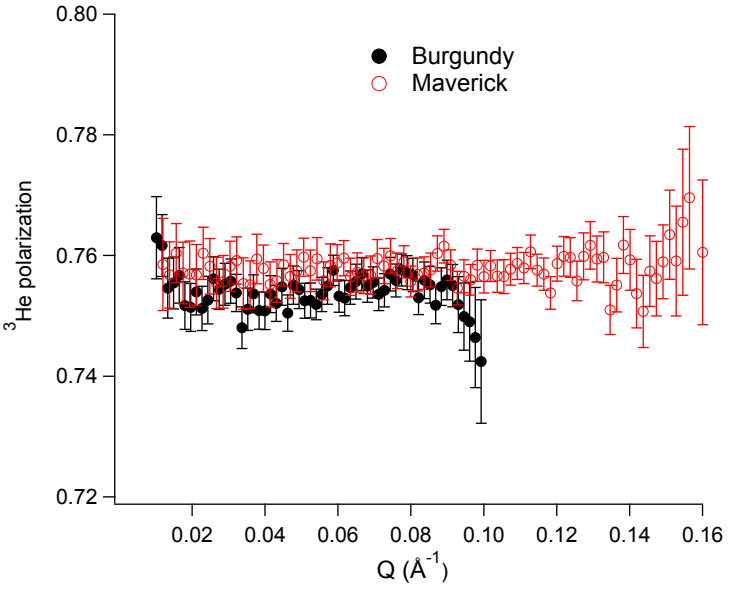

Fig. 6. Path length variation in ^{3}He polarization as a function of the wave vector transfer. The ^{3}He polarization was obtained at each scattering angle using Eq. 3 and the opacity variation in Fig. 3 for the cells Burgundy and Maverick. The ^{3}He polarizations were 0.754 and 0.757 for the cells Burgundy and Maverick obtained by fitting the polarization plot to a constant.

6. Conclusions

In summary, we have characterized and modeled the two-dimensional neutron path variation in opacity, transmission through polarized ^{3}He cells, and neutron polarization yielded from a ^{3}He NSF when large divergent scattered neutron beams pass through the end windows of the cylindrical cells. The experiment utilizes a large two-dimensional SANS position-sensitive detector and a strong coherent scatterer. The path length variations in opacity and transmission are about 10 % and 8 %, respectively, from the cell center to the edge in the configuration studied here and depend on the cell geometry and the instrument setup. The neutron polarization resulting from a ^{3}He NSF is not sensitive to the path length variation (about 1 %). Although the effect is not large, it should be corrected in polarization efficiency correction software when ^{3}He NSFs are used on the neutron beam-line. The path length variation effect can be cancelled if one appropriately locates the ^{3}He cell close to the sample. We have implemented the path length correction in the polarization efficiency correction software we have developed for various instruments (TAS and MACS) at the NCNR. We plan to implement the correction into the SANS and reflectometry software. We plan to characterize and model the path length variation in polarized neutronic performance.

7. Acknowledgments

The authors thank J. Anderson of the NIST Optical Shop for assistance with cell fabrication. We wish to thank K.L. Krycka, and C. Gagnon for their assistance for the NG-3 SANS instrument setup. We benefitted from valuable discussions with T.R. Gentile. The work utilized facilities supported in part by the National Science Foundation under Agreement No. DMR-0944772.

References

[1] W.C. Chen *et al.*, Physica B **397**, 168 (2007).
[2] K.L. Krycka *et al.*, Physica B **404**, 2561 (2009).
[3] W.C. Chen *et al.*, Physica B **404**, 2663-2666 (2009).
[4] E. Babcock *et al.*, Physica B **406**, 2448 (2011).
[5] W. C. Chen *et al.*, Rev. Sci. Instrum. **75**, 3256-3263 (2004).
[6] W.T. Lee *et al.*, J. Phys.: Conf. Series **251**, 012086 (2010).
[7] K.H. Andersen *et al.*, Physica B **404**, 2652-2654 (2009).
[8] C.B. Fu *et al.*, Physica B **406**, 2419-2423 (2011).
[9] GE Lighting Component Sales, Bldg. 315D, 1975 Noble Rd., Cleveland, OH 44117. Certain trade names and company products are mentioned in the text or identified in an illustration in order to adequately specify the experimental procedure and equipment used. In no case does such identification imply recommendation or endorsement by the National Institute of Standards and Technology, nor does it imply that the products are necessarily the best available for the purpose.
[10] N.R. Newbury, A.S. Barton, G.D. Cates, W. Happer, and H. Middleton, Phys. Rev. A **48** 4411 (1993).
[11] W.C. Chen *et al.*, J. Phys.: Conf. Series **294**, 012003 (2011).
[12] C.J. Beecham *et al.*, Physica B **406**, 2429 (2011).
[13] T. R. Gentile *et al.*, J. Appl. Cryst. **33**, 771 (2000).
[14] K.L. Krycka *et al.*, Phys. Rev. Lett. **104**, 207203 (2010).
[15] C. Dufour *et al.*, Phys. Rev. B **84**, 064420 (2011).
[16] M. Ramazanoglu *et al.*, Phys. Rev. Lett. **107**, 207206 (2011).
[17] K.L. Krycka *et al.*, J. Appl. Phys. **109**, 07B513 (2011).
[18] M. Laver *et al.*, Phys. Rev. Lett. **105**, 027202 (2010).
[19] T.E. Chupp *et al* Nucl. Instrum. Meth. A **574** 500 (2007).
[20] http://www.ill.eu/science-technology/neutron-technology-at-ill/optics/3he-spin-filters/3he-cells/.
[21] http://www.smallangles.net/wgwiki/index.php/Glassy_Carbon_Round_Robin.
[22] C. J. Glinka *et al.*, J. Appl. Cryst. **31**(3), 430 (1998).